Angiogenesis (2022) 25:331–342
https://doi.org/10.1007/s10456-022-09836-7

BRIEF COMMUNICATION

NRAS^{Q61R} mutation in human endothelial cells causes vascular malformations

Elisa Boscolo[1,2,3] · Patricia Pastura[4] · Sandra Schrenk[2,3] · Jillian Goines[2,3] · Rachael Kang[2,3] · Devin Pillis[2,3] · Punam Malik[1,2,3] · Timothy D. Le Cras[1,4]

Received: 18 October 2021 / Accepted: 22 March 2022 / Published online: 7 April 2022

Abstract

Somatic mutations in NRAS drive the pathogenesis of melanoma and other cancers but their role in vascular anomalies and specifically human endothelial cells is unclear. The goals of this study were to determine whether the somatic-activating NRAS^{Q61R} mutation in human endothelial cells induces abnormal angiogenesis and to develop in vitro and in vivo models to identify disease-causing pathways and test inhibitors. Here, we used mutant NRAS^{Q61R} and wild-type NRAS (NRAS^{WT}) expressing human endothelial cells in in vitro and in vivo angiogenesis models. These studies demonstrated that expression of NRAS^{Q61R} in human endothelial cells caused a shift to an abnormal spindle-shaped morphology, increased proliferation, and migration. NRAS^{Q61R} endothelial cells had increased phosphorylation of ERK compared to NRAS^{WT} cells indicating hyperactivation of MAPK/ERK pathways. NRAS^{Q61R} mutant endothelial cells generated abnormal enlarged vascular channels in a 3D fibrin gel model and in vivo, in xenografts in nude mice. These studies demonstrate that NRAS^{Q61R} can drive abnormal angiogenesis in human endothelial cells. Treatment with MAP kinase inhibitor U0126 prevented the change to a spindle-shaped morphology in NRAS^{Q61R} endothelial cells, whereas mTOR inhibitor rapamycin did not.

Keywords Vascular Anomaly · Vascular Malformation · RASopathies · Lymphatic anomaly · Kaposiform lymphangiomatosis

Introduction

Mutations that activate RAS/MEK/ERK or inactivate suppressors of this important pathway are commonly found in a variety of cancer types and are now being targeted for cancer therapy [1]. The activating NRAS^{Q61R} mutation is common in difficult to treat melanomas [2]. Recently, somatic NRAS mutations have begun to be identified in various vascular anomalies [3]. Notably, 10% of patients with pyogenic granuloma (PG), a vascular neoplasm, have non-inherited NRAS^{Q61R} mutation [4]. In other types of PG, KRAS and HRAS-activating mutations have been found [4, 5] leading to the possibility that hyperactive RAS/MAPK signaling is a common mechanism. The NRAS^{Q61R} mutation has also been found in patients with kaposiform lymphangiomatosis (KLA)[6] suggesting that RAS/MAPK/ERK may be an important pathway in this aggressive lymphatic malformation characterized by overgrowth of dysfunctional vessels and spindled endothelial cells. A recent case study also identified a somatic mutation in Casitas B-lineage lymphoma

Patricia Pastura and Sandra Schrenk have contributed equally to this work.

✉ Elisa Boscolo
elisa.boscolo@cchmc.org

✉ Timothy D. Le Cras
tim.lecras@cchmc.org

1 Department of Pediatrics, University of Cincinnati College of Medicine, Cincinnati, OH, USA

2 Division of Experimental Hematology and Cancer Biology, Cincinnati Children's Hospital, Cincinnati, OH, USA

3 Cancer and Blood Diseases Institute, Division of Hematology, Cincinnati Children's Hospital, Cincinnati, OH, USA

4 Division of Pulmonary Biology, Cincinnati Children's Hospital, Center, 3333 Burnet Avenue, Cincinnati, OH 45229-3039, USA

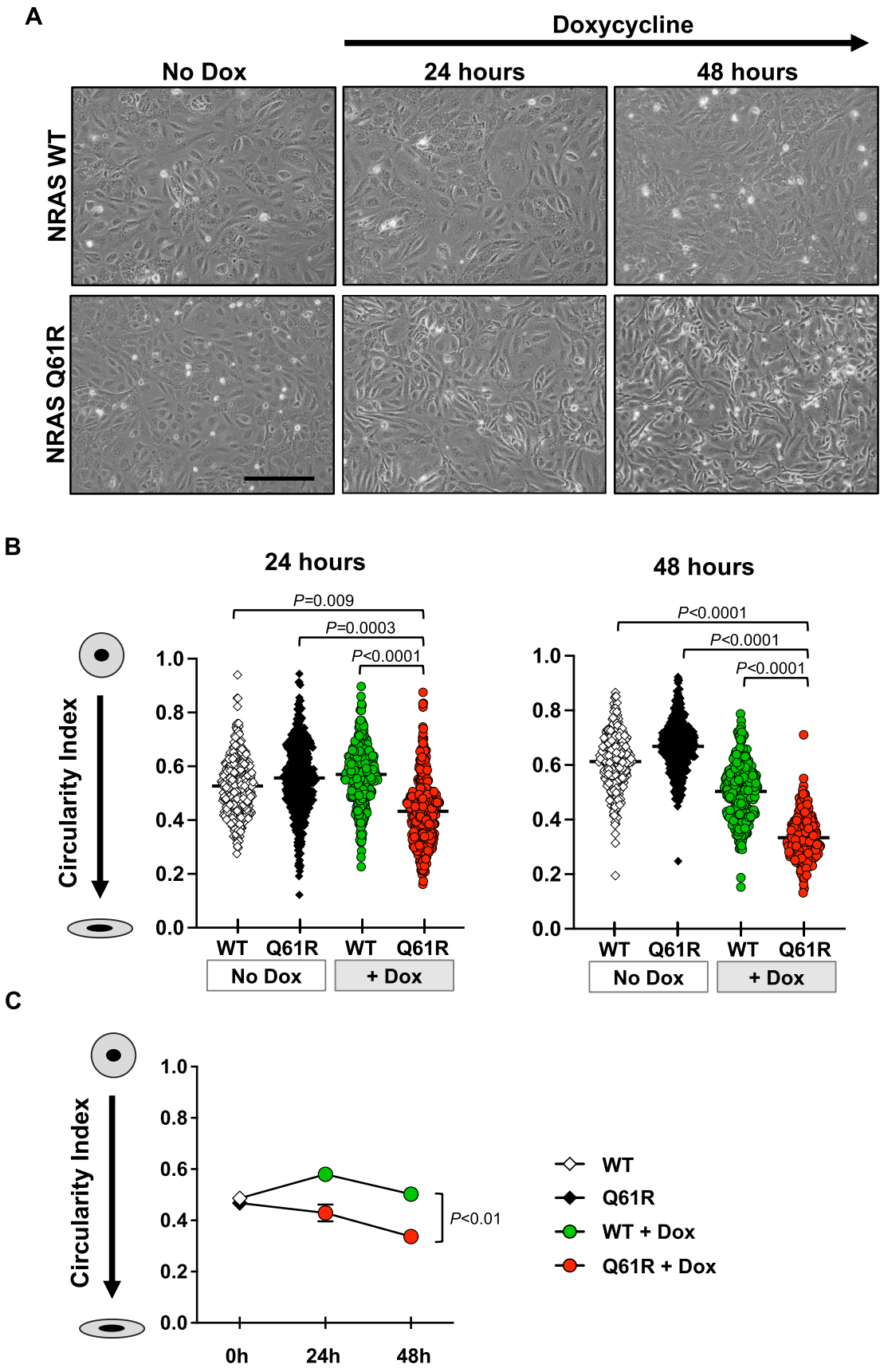
A
Doxycycline
No Dox
24 hours
48 hours
NRAS WT
NRAS Q61R
B
24 hours
48 hours
P=0.009
P=0.0003
P<0.0001
P<0.0001
P<0.0001
P<0.0001
Circularity Index
1.0
0.8
0.6
0.4
0.2
0.0
WT Q61R WT Q61R
No Dox
+ Dox
C
Circularity Index
P<0.01
0h
24h
48h
WT
Q61R
WT + Dox
Q61R + Dox

◂**Fig. 1** Morphology of human endothelial progenitor cells (EPC)-expressing $NRAS^{WT}$ and $NRAS^{Q61R}$. Panel **A**: Representative images of EPC monolayer with no Doxycycline (No Dox) and 24 and 48 h after addition of Doxycycline to the cell culture media. $n=4$ independent experiments. Scale bar = 200 µm Panel **B and C**: Circularity index measurements for EPC-expressing $NRAS^{WT}$ and $NRAS^{Q61R}$ in No Dox and Dox-containing media at 24 and 48 h. In B, measurements for each cell is shown. One-way Anova followed by Tukey's test for multiple comparisons. In C, data points are mean ± SD; $n=4$ independent experiments. Two-way Anova followed by Bonferroni test for multiple comparisons, p values are at 24 and 48 h

(CBL) proto-oncogene in one KLA patient who was effectively treated with a MEK inhibitor [7].

Hence, an emerging concept is that dysfunctional RAS signaling in endothelial cells may play a role in different types of vascular anomalies. However, while the pathways and effectors downstream of $NRAS^{Q61R}$ in melanoma have been identified, the pathways that this mutation activates in endothelial cells are still largely unexplored. To address this question, we generated lentiviral constructs with doxycycline-regulated $NRAS^{Q61R}$ or NRAS wild type ($NRAS^{WT}$). Each construct was introduced into human endothelial progenitor cells (EPC). EPCs isolated from human cord blood are excellent for modeling angiogenesis in vitro and in vivo[8]. $NRAS^{Q61R}$ and $NRAS^{WT}$-expressing EPC were characterized in vitro and in vivo. Changes in EPC morphology, proliferation, migration, and downstream signaling pathways were assessed. Vascular morphogenesis was compared in a 3D in vitro angiogenesis model. A xenograft model was generated by taking $NRAS^{Q61R}$ and $NRAS^{WT}$ EPC enrobed in Matrigel® and injecting the cells under the skin of nude mice fed a doxycycline-containing diet. In a proof-of-concept study, inhibitors of the MAP Kinase and mTOR signaling pathways were tested to determine if they blocked changes in cell morphology.

Materials & methods

Generation of lentiviral constructs

DNA sequences-encoding $NRAS^{Q61R}$ and $NRAS^{WT}$ were subcloned into lentiviral vector pCW from Addgene (see Supplemental Fig. S1 for construct maps). The lentiviral constructs were packaged into viral particles and viral titer determined.

Cell culture, transduction and selection

Human endothelial progenitor cells (EPC) isolated from human cord blood were obtained from StemBiosys (CELLvo EPC). EPCs were plated onto fibronectin-coated plates and cultured in endothelial growth medium (EGM2) with 20% fetal bovine serum (FBS) (Lonza) and 1% penicillin–streptomycin–glutamine. Viral particles containing pCW-$NRAS^{Q61R}$ or pCW-$NRAS^{WT}$ were added to the EPC at a multiplicity of infection of 1. Hexadimethrine bromide (8 µg/ml) was also added to the media to increase the efficiency of infection. After 24 h, the media were replaced with puromycin-containing (0.5 µg /ml) media to select for cells that had taken up the constructs. The cells were cultured for 10 days in puromycin-containing medium and frozen back for future use. Doxycycline (Dox) was added to the media to induce $NRAS^{Q61R}$ or $NRAS^{WT}$ expression (1–2 µg/ml). For inhibitor studies, U0126 (10 µM) or rapamycin (15 nM), or vehicle (0.05% DMSO) was added and cell morphology (Circularity index) of the cells was measured at 48 h.

Cell morphology, proliferation & migration

Morphology of $NRAS^{Q61R}$ and $NRAS^{WT}$ EPC was photographed before (No Dox) and 24 and 48 h after addition of Dox. Circularity index of the cells, which is equal to 1 when cells are spheric and 0 when cell shape is spindled, was measured using ImageJ [9]. For proliferation analysis, cells were plated onto fibronectin-coated 96-well plates at 6000 cells per well with > 8 replicates. Cell growth was monitored for 3 days using an IncuCyte® ZOOM Live Cell Imaging System (Essen BioScience). Percentage of cell confluence was calculated to determine the cell growth rate. SRB assay was also used to assess cell proliferation. For the migration assay, cells were seeded at 1×10^5 cells/cm^2 into an Ibidi Culture-Insert 2 Well system (Ibidi) and allowed to grow to confluency. The cells were pretreated with 2 mM hydroxyurea (Sigma) for 4 h to inhibit proliferation before creating the gap—The culture insert was gently removed using sterile tweezers, leaving a cell-free gap of approximatively 500 µm width, and medium was replaced with fresh medium containing 2 mM hydroxyurea. Images of the cell-free gap were captured at 0, 2, 4, 6, and 8 h using an EVOS-imaging system (Invitrogen). The cell-free area was measured over time using ImageJ software, and the value was expressed as percentage of the initial cell-free area (% gap closure area).

Western blot analysis of signaling pathways

Cell lysates were prepared after 2, 7, and 14 days of Dox treatment or from no Dox control plates. 30 µg of protein was loaded onto a 4–12% Bis/Tris polyacrylamide gel. After separation of the proteins by electrophoresis, the proteins were transferred to a PVDF membrane by western transfer. The membranes were blocked in 5% nonfat dry milk overnight at 4 °C. Primary antibodies against $NRAS^{Q61R}$ (227658, 1:400; Abcam), NRAS (77392, 1:1000; Abcam), phospho-ERK (4370, 1:2000; Cell Signaling), ERK (9102, 1:1000; Cell Signaling), phospho-AKT (Ser473)(4060,

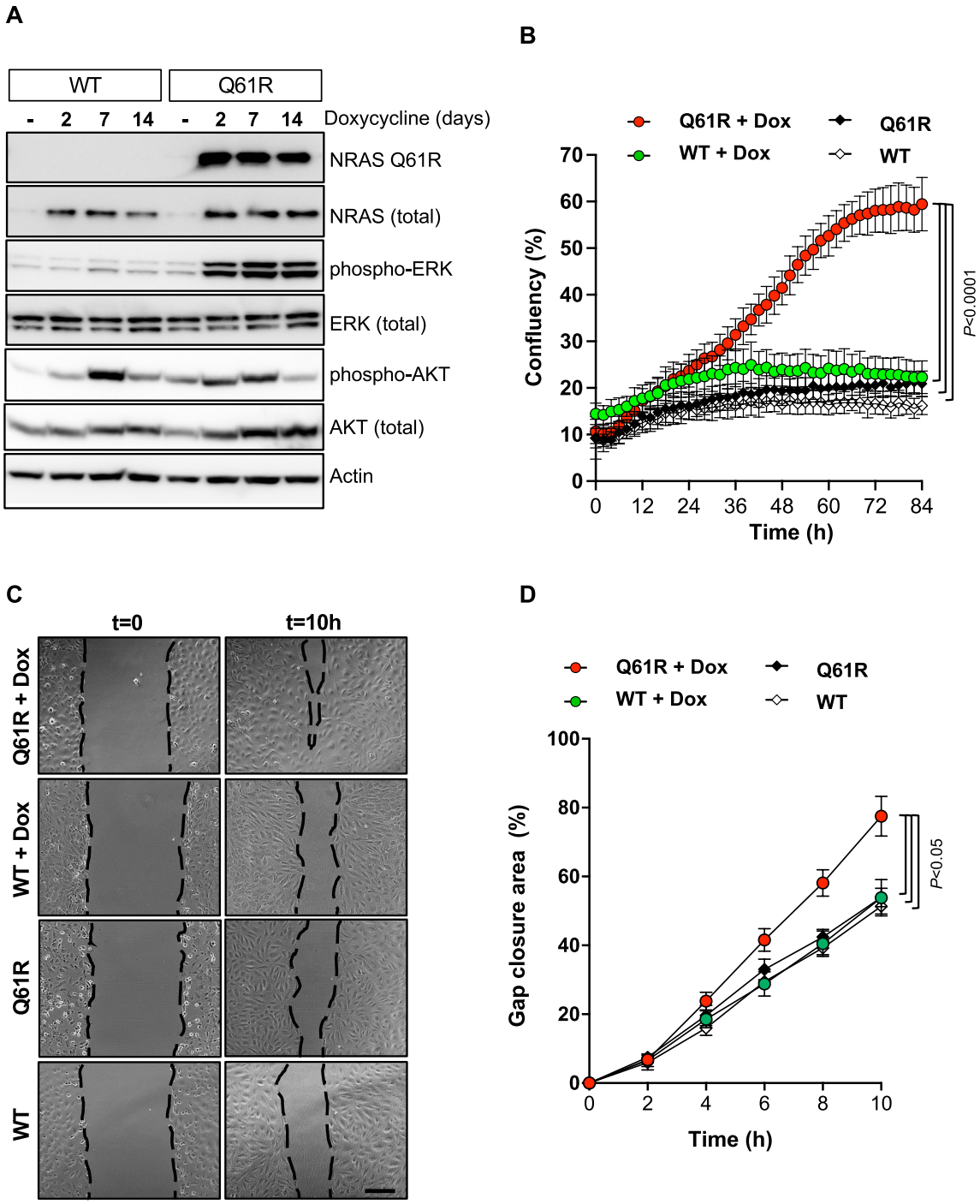

Fig. 2 Signaling pathways and angiogenic properties of human endothelial progenitor cells (EPC) expressing $NRAS^{WT}$ and $NRAS^{Q61R}$. Panel **A**: Cell lysates were analyzed 2, 7 and 14 days after doxycycline (Dox) was added to the cell culture media. Antibodies specific to the mutated form of NRAS ($NRAS^{Q61R}$), wild-type NRAS (total), phospho-ERK, phospho-AKT Ser473, total ERK, total AKT, and actin were used. Representative blot of $n=3$ independent repeats. Panel **B**: Proliferation of endothelial cells was measured using an Incucyte® system in endothelial basal medium (EBM2) containing 20% fetal bovine serum (FBS). Data points are mean ± SD; $n=8$ wells. Two-way Anova followed by Bonferroni test for multiple comparisons. P value < 0.0001 for times ≥ 36 h. **Panel C**: Representative images of migration of endothelial cells at $t=0$ and $t=10$ h after the wound was made. Scale bar: 200 µm. Panel **D**: Migration area of endothelial cells was measured every 2 h from 0 to 10 h after creating the gap. Percentage gap closure was determined. Data points are mean ± SD; shown is one representative of $n=2$ independent experiments with 3–4 wells analyzed. Two-way Anova followed by Bonferroni test for multiple comparisons. *P* value < 0.05 at 6, 8, 10 h

1:2000; Cell Signaling), AKT (9272, 1:1000; Cell Signaling), phospho-S6 Ser 235/236 (4858, Cell Signaling), S6 (2217, Cell Signaling), and actin (C4, 1:10,000; Seven Hills Bioreagents) were added for 1 h. After washing 5 times in TBST for 5 min, secondary antibodies (anti-rabbit, anti-goat, anti-mouse; Calbiochem) were added for 1 h at room temperature. Blots were washed, and Millipore Immobilon was used for the chemiluminescent detection. Images of blots were obtained using the LAS 4000 imaging system (Fujifilm).

3D lumen formation assay

3D lumen formation assay was performed as previously described [10]. Briefly, Cytodex® 3 microcarrier beads (Sigma) were incubated with $NRAS^{Q61R}$ or $NRAS^{WT}$ EPC at a concentration of 400 cells/ bead for 4 h at 37 °C. The following day, coated beads were resuspended in 2 mg/mL of fibrinogen (Sigma) solution containing 0.15 U/mL of aprotinin (Sigma) at a concentration of 500 beads/ml. Then 0.625 U/mL of thrombin (Sigma) and 0.5 ml beads/fibrinogen suspension were added per well of a 24-well plate and incubated at 37 °C for 20 min to allow fibrin clotting. The gels were overlaid with human dermal fibroblasts at 2×10^4 cells/well and cultured in EBM2 supplemented with 20% FBS and with or without 2ug/mL doxycycline. Medium was replaced every other day. Images were acquired at indicated time points using the EVOS cell-imaging system (Invitrogen), and the vascular area was analyzed with Fiji (Image J) software [11]. Immunofluorescent staining on fibrin gels was performed upon overnight fixation in 4% paraformaldehyde at 4 °C. Fibrin gels were incubated overnight at 4 °C with biotinylated UEA-1 (20 µg/ml, Vector Laboratories) followed by incubation with Texas Red® Streptavidin (Vector Laboratories; 5 µg/ml) for 4 h at room temperature. Nuclei were visualized with DAPI (4′,6-diamidino-2-phenylindole). Z-stack images were acquired on a Nikon A1R laser-scanning confocal microscope, and surface reconstruction of vascular structures was performed using Imaris Imaging Analysis software (Bitplane).

Generation of mouse xenograft model & evaluation of vascular growth

All animal experiments were approved by the Institutional Animal Care and Use Committee at Cincinnati Children's Hospital in an Association for Assessment and Accreditation of Laboratory Animal Care-approved facility. Following expansion in tissue culture, 2.5×10^6 human EPCs expressing $NRAS^{Q61R}$ or $NRAS^{WT}$ were exposed to doxycycline for 48 h (no doxycycline as control) and suspended in 200 µL Matrigel® (Corning) and subcutaneously injected into both flanks of 6 to 7-week-old male athymic nu/nu male mice (Envigo). Lesions were dissected and weighed 8 days later, then fixed in 4% paraformaldehyde, and paraffin embedded. Paraffin Sects. (5 µm) were stained with hematoxylin and eosin (H&E). Five random images per section were captured using an EVOS microscope (Life Technologies), and vascular area (% of field area) was quantified using ImageJ software as previously reported [12].

Immunohistochemistry

Paraffin sections of the xenografts were stained with UEA I (Ulex europaeus Agglutinin I;1:100, Vector Laboratories). This was followed by peroxidase-conjugated secondary antibody and staining with diaminobenzidine peroxidase (horseradish peroxidase) substrate (Vector Laboratories). Slides were counterstained using hematoxylin (Vector Laboratories). Images were captured using a Nikon microscope.

Immunofluorescence staining for VE-cadherin

Immunofluorescence staining was performed with an antibody to VE-cadherin (555661, 1:50; BD Pharmingen) was performed on fixed monolayers incubated overnight at 4C. Secondary antibody was Alexa Fluor 488 anti-mouse labeled IgG (A21121, 1:200, Invitrogen). Slides were covered with a coverslip with Prolong Gold with DAPI (Invitrogen), and images were acquired on Nikon A1R laser-scanning confocal microscope.

Statistical analysis

Data are expressed as mean ± standard deviation (SD) and analyzed by Welch's *t* test or parametric one-way ANOVA after normal distribution, and equal variance was assessed. One-way ANOVA with post hoc (Tukey or Fisher) test was used for multiple comparisons. For data with correlated observations, a repeated measures two-way ANOVA was used, followed by post hoc (Bonferroni) test. All calculations were performed using GraphPad Prism. Differences were considered significant for P value < 0.05.

Results

Expression of $NRAS^{Q61R}$ in human endothelial cells induces altered morphology and hyperactive MAPK pathway

Lentiviral constructs were generated with doxycycline-inducible expression of mutant $NRAS^{Q61R}$ or $NRAS^{WT}$ as a control (Supplemental Fig. S1). Each construct was transduced into EPC. EPCs were grown in endothelial growth medium, and morphology was analyzed 24 h and 48 h after

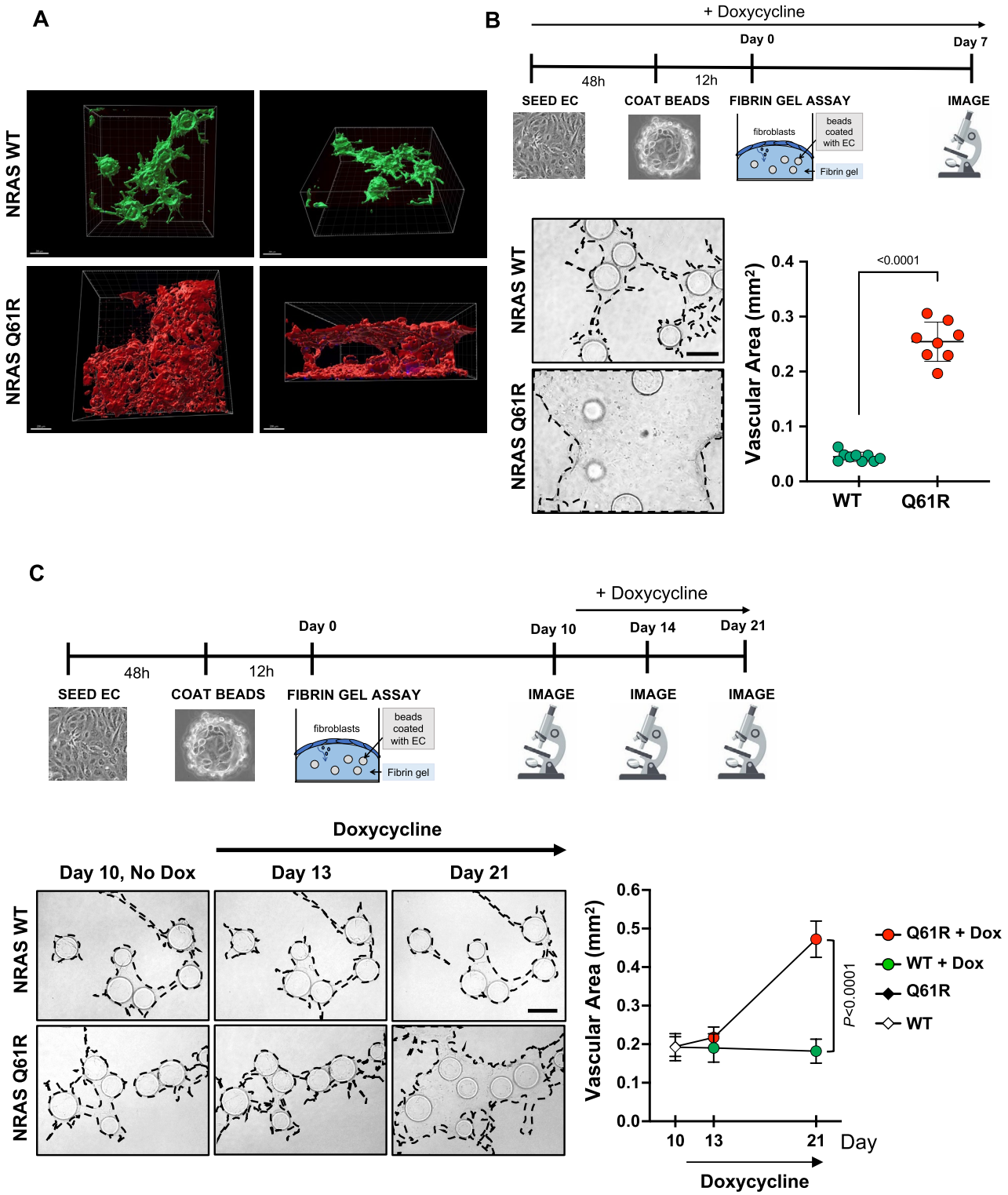

doxycycline was added to the medium. Cell shape in EPC-expressing NRAS^{Q61R} overtly changed from the typical endothelial cobblestone-like morphology to an elongated/spindled shape (Fig. 1A and Supplemental Fig. S2). The morphological change was analyzed by measuring the circularity index which equals 1 when cells are spheric and 0 when cell shape is spindled. The circularity index was significantly lower ($p < 0.0001$ at both 24 and 48 h) in EPC-expressing NRAS^{Q61R} compared to NRAS^{WT} (Fig. 1B). Furthermore, in EPC-expressing NRAS^{Q61R}, the circularity

◂**Fig. 3** Human endothelial progenitor cells (EPC)-expressing $NRAS^{Q61R}$ form enlarged vascular structures in a 3D lumen formation assay. Panel **A**: Imaris-generated 3D structural models of vascular channels formed by human EPC-expressing $NRAS^{WT}$ and $NRAS^{Q61R}$ stained for Ulex europaeus agglutinin-I (UEA) on day 7. Scale Bars = 200 μμ. Panel **B**: Experimental protocol schematic (top), Doxycycline was added 48 h prior starting the 3D lumen formation assay. Representative 2D images of vascular structures (bottom, left) and quantification of vascular area (normalized by bead number) at day 7 (bottom, right). Data points are mean ± SD; $n = 3$ independent experiments. Welch's t test. Panel **C**: Experimental protocol schematic, Doxycycline was not added until day 10 (top). Representative 2D images of vascular structures (bottom, left) and quantification of vascular area at days 10, 13, and 21 (bottom, right). Data points are mean ± SD; $n = 3$ independent experiments. Two-way Anova followed by Bonferroni test for multiple comparisons. *P* value < 0.0001 at day 21. Scale Bars in Panel B and C = 100 μμ

index decreased at 24 h and 48 h, when compared to no Dox ($t = 0$ h) (Fig. 1C).

Next, to confirm expression of $NRAS^{Q61R}$ and $NRAS^{WT}$, we performed immunoblotting with an antibody specific for the mutant $NRAS^{Q61R}$ and an antibody that detects both $NRAS^{WT}$ and $NRAS^{Q61R}$, hereafter referred to as total NRAS. Upon doxycycline administration for 2, 7, and 14 days, $NRAS^{Q61R}$ expression was elevated, and ERK and AKT (Ser473) were phosphorylated (Fig. 2A). The proliferative and migratory capacity of EPC expressing the mutant $NRAS^{Q61R}$ or $NRAS^{WT}$ were measured. Using an Incucyte® system, $NRAS^{Q61R}$ EPC (with doxycycline) showed a higher proliferation rate than $NRAS^{WT}$ EPC (on doxycycline) and no dox $NRAS^{Q61R}$ EPC (Fig. 2B). Proliferation was also measured using SRB (Sulforhodamine B) assay, and similar results were seen (Supplemental Fig. S3). Cell migration was measured with a gap closure assay upon removal of an insert that generates a gap in the cell monolayer. EPC-expressing $NRAS^{Q61R}$ (treated with doxycycline) migrated faster and closed the gap faster than $NRAS^{WT}$ (with and without doxycycline) (Fig. 2C, D). These data show that EPC-expressing $NRAS^{Q61R}$ developed an abnormal morphology, increased p-ERK, enhanced proliferation, and migration compared to $NRAS^{WT}$ cells.

Expression of $NRAS^{Q61R}$ in human endothelial cells induces formation of dilated vascular channels in a 3D fibrin gel lumen formation assay

To investigate the vasculogenic potential of EPC-expressing $NRAS^{Q61R}$, we employed an in vitro 3D (three-dimensional) fibrin gel system [10] that we previously employed to mimic venous malformation morphogenesis [13]. When control $NRAS^{WT}$ human EPC-coated beads were embedded in fibrin gels topped with fibroblasts, they formed longitudinal lumenized vessels (Fig. 3A). Conversely, EPC-expressing $NRAS^{Q61R}$ formed dilated hollow vascular structures (Fig. 3A and Supplemental Video S1-2).

To further determine the consequences of the $NRAS^{Q61R}$ expression on the lumen formation, we pretreated cell monolayer with doxycycline for 48 h prior embedding the cells in the 3D fibrin gel, and doxycycline was added to the medium on top of the gel. At day 7, analysis revealed that $NRAS^{Q61R}$ EPC formed dilated vascular channels and showed significantly increased vascular area compared to $NRAS^{WT}$ ($p < 0.0001$) (Fig. 3B).

To model changes in lumen morphogenesis in a normal vessel – upon expression of $NRAS^{Q61R}$, we performed the 3D lumen formation assay with $NRAS^{Q61R}$ and control $NRAS^{WT}$ EPC without exposing cells to doxycycline. By day 10 without doxycycline administration, lumens formed as in normal EPC (Fig. 3C). After day 10, doxycycline was added to the gel and correlated analysis at days 13 and 21 revealed vascular area expansion due to $NRAS^{Q61R}$ expression, while area did not change with expression of $NRAS^{WT}$. These data show that EPC-expressing $NRAS^{Q61R}$ in the 3D fibrin gel can phenocopy dilated vascular lesions as detected in vascular anomaly patients with hyperactive NRAS mutations.

Generation of a murine xenograft model for vascular anomalies with human endothelial mutant $NRAS^{Q61R}$ cells

Human EPC-expressing $NRAS^{WT}$ or $NRAS^{Q61R}$ were expanded in doxycycline-containing cell culture medium, suspended in 200μl of Matrigel® and subcutaneously injected into immune-deficient mice fed with doxycycline-containing chow (Fig. 4A). We evaluated if they could recapitulate the histological features of vascular anomalies with hyperactive NRAS mutations. Murine lesion xenograft explants (plugs) containing doxycycline-treated $NRAS^{Q61R}$ EPC were visibly vascularized on day 8 and their weight was significantly ($p < 0.05$) higher compared to the other experimental control groups (Fig. 4B). Hematoxylin and eosin staining of xenograft sections revealed numerous dilated vascular channels in mice injected with EPC-expressing $NRAS^{Q61R}$ on Dox, while EPC-expressing $NRAS^{WT}$ (treated with doxycycline), $NRAS^{Q61R}$, and $NRAS^{WT}$ not on Dox generated only minimal vascularization (Fig. 4C). The vascular area in doxycycline-treated $NRAS^{Q61R}$ EPC-xenograft lesions was significantly higher than control EPC xenografts ($p < 0.05$) (Fig. 4C), and in general, vessels were bigger in size compared to the control groups (Supplemental Fig. S4). Lesional ectatic channels in the xenografts showed binding to the endothelial human-specific lectin Ulex europaeus agglutinin-I (UEAI) (Fig. 4D). This confirms that vascular channels in the xenografts were mostly generated by the human EPC rather than invading mouse vessels. All together, these results show that $NRAS^{Q61R}$ expression

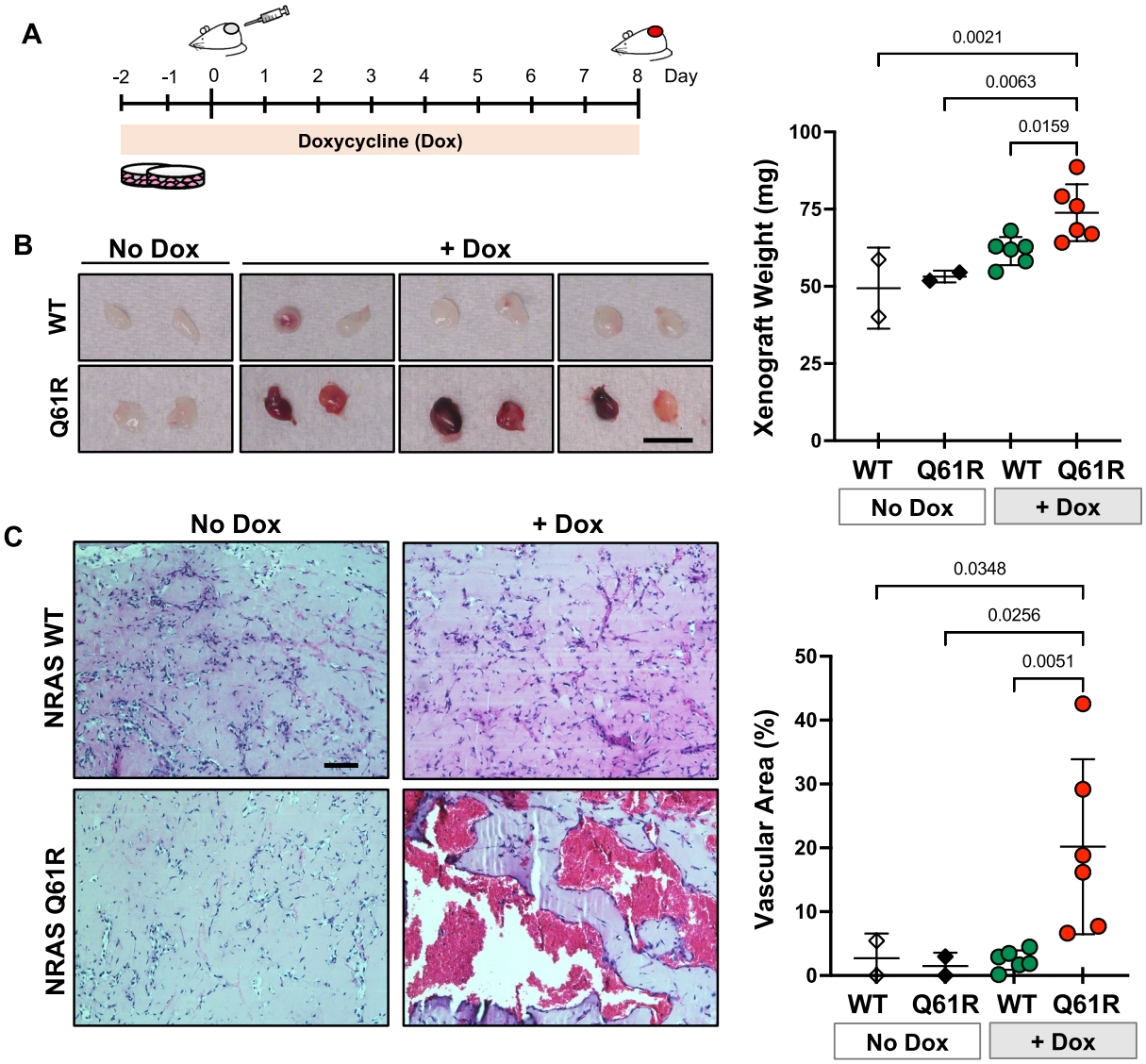
A
-2 -1 0 1 2 3 4 5 6 7 8 Day
Doxycycline (Dox)
B
No Dox
+ Dox
WT
Q61R
Xenograft Weight (mg)
0.0021
0.0063
0.0159
100
75
50
25
0
WT Q61R WT Q61R
No Dox
+ Dox
C
No Dox
+ Dox
NRAS WT
NRAS Q61R
Vascular Area (%)
0.0348
0.0256
0.0051
50
40
30
20
10
0
WT Q61R WT Q61R
No Dox
+ Dox
D
No Dox
+ Dox
UEAI
NRAS WT
NRAS Q61R

◂**Fig. 4** Human endothelial progenitor cells (EPC)-expressing $NRAS^{Q61R}$ form enlarged and perfused vascular structures in a murine xenograft model. Panel **A**: Experimental protocol showing time of cell injection and Doxycycline treatment period, and time of harvest of xenograft plugs. Panel **B**: Pictures and graph of weight measurements of the xenograft plugs after removal from mice at day 8. Data points are mean ± SD; $n = 2–6$ mice with 2 plugs. One-way Anova followed by Fisher test for multiple comparisons. Panel **C**: Histology of xenograft plugs after removal from mice at day 8. Tissue sections were stained with hematoxylin and eosin. Graph shows vascular area measured from histology. One-way Anova followed by Fisher test for multiple comparisons. Panel **D**: Immunostaining of xenograft plug sections for Ulex europaeus agglutinin-I (UEA) that is expressed by human endothelial cells and not mouse endothelial cells. Scale bars = 1 cm in B, 100 µm in C and D

induces formation of enlarged vessels using this xenograft model.

Treatment of mutant $NRAS^{Q61R}$ endothelial cells with MAPK/ERK and mTOR inhibitors

A proof-of-concept study was performed to verify that $NRAS^{Q61R}$ EPC could be used to determine the role of signaling pathways and to test drugs. First, we verified that the MAPK/ERK inhibitor U0126 at 10 µM prevented the phosphorylation of ERK and that mTOR inhibitor rapamycin at 15 nM reduced phosphorylation of S6. These two drugs were effective on both $NRAS^{Q61R}$ and $NRAS^{WT}$ EPC (Fig. 5A). Next, measurement of the cell shape was performed with doxycycline and U0126 or rapamycin for 48 h. Analysis of cell circularity index showed that U0126 prevented the shift to a spindle-shaped morphology in the $NRAS^{Q61R}$ EPC, whereas mTOR inhibitor rapamycin did not (Fig. 5B, C). These results show that $NRAS^{Q61R}$ expression induces cell shape change towards a spindle morphology and that MAPK/ERK inhibition is effective at preventing this change. This would suggest MAPK/ERK pathway is involved in the cell shape change in the NRAS mutant cells.

Discussion

Somatic-activating mutations in RAS or loss-of-function mutations in genes that suppress RAS signaling are common in tumors [1] and have now been identified in patients with vascular anomalies [3–5]. While the $NRAS^{Q61R}$ mutation has been found in tissue from PG and KLA patients [4, 6], its role in the pathogenesis of these diseases is unclear. Whether the mutation by itself is sufficient to drive the disease or additional mutations or environmental factors are needed is unknown. Our results show that $NRAS^{Q61R}$ expression in human endothelial cells induces abnormal cell morphology and increases the rate of proliferation and migration in vitro. Our in vitro angiogenesis model lends further support as $NRAS^{Q61R}$-expressing endothelial cells formed enlarged abnormal structures compared to $NRAS^{WT}$ cells. Furthermore, in a xenograft model, $NRAS^{Q61R}$ endothelial cells formed enlarged channels with increased vascular area and size.

Our studies showed that expression of $NRAS^{Q61R}$ induced a spindle-shaped endothelial cell morphology that is seen in the histopathology of KLA patients [14]. Changes in cell morphology to acquire elongations or spindled shape have also been reported in endothelial cells-expressing PIK3CA or TEK constitutive active mutations [15] modeling venous malformation and in a SMAD4 loss-of-function murine model of arteriovenous malformations [16]. It is possible that these morphological changes are a pre-requisite for the formation of vascular malformations with dilated vascular channels. $NRAS^{Q61R}$ endothelial cells had enhanced proliferation and migration, as was MAPK/ERK and PI3 Kinase/AKT pathway activation. These are not unexpected given the role of these key signaling pathways in cell morphology, division, and migration. In a 3D in vitro angiogenesis model, $NRAS^{Q61R}$ endothelial cells formed abnormally large channels compared to $NRAS^{WT}$ cells which formed narrow-hollowed longitudinal channels. Of note, a recent study showed abnormal morphogenesis and failure to form elongated tubes in endothelial cells-expressing mutant $HRAS^{V12}$ [17]. A similar in vitro 3D model for venous malformation was successfully used to establish the efficacy of PI3K/mTOR inhibitors in preventing lumen formation and enlargement [18]. These 3D systems could be employed in the future as a tool to study the mechanisms leading to malformed vascular lumens and to screen for drugs that could normalize the $NRAS^{Q61R}$ phenotype.

When injected under the skin of nude mice the $NRAS^{Q61R}$ endothelial cells formed enlarged bloody channels not unlike the pathology of lesions in PG and KLA patients [14]. While animal models for vascular anomalies with the $NRAS^{Q61R}$ mutation have not been reported yet, other groups have recently modeled in mouse vascular anomalies associated with KRAS activating mutations [19, 20]. Somatic-activating mutations in KRAS have been found in patients with brain arteriovenous malformations and targeted endothelial expression of $KRAS^{G12D}$ in mice generated a mouse model with pathology similar to the patients [19]. The $KRAS^{G12V}$ mutation has been found in Gorham-Stout Disease (GSD), where ectopic overgrowth of lymphatic vessels into the bones is associated with bone loss–this was modeled using $Prox1\text{-}Cre^{ERT2}$ mice to target $KRAS^{G12V}$ and mimicked many key features of human GSD [20].

Although signaling of the RAS family members is similar because of the highly conserved effector domains, the specificity of the different isoforms is just starting to be explored in the vascular endothelium. Clearly, RAS signaling is

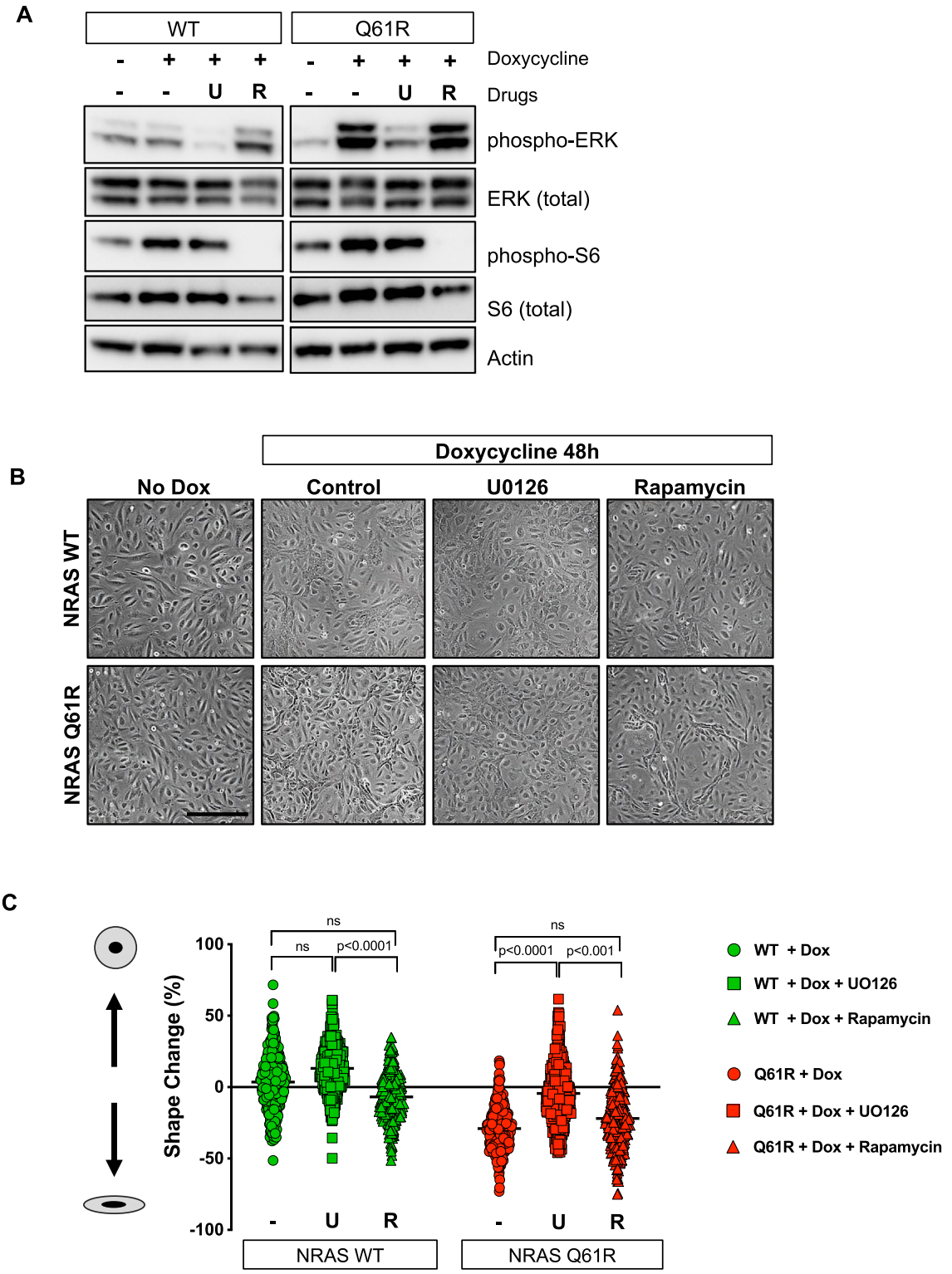

Fig. 5 Treatment of endothelial progenitor cells (EPC) expressing $NRAS^{Q61R}$ with MAPK/ERK and mTOR inhibitors. Panel **A**: Western blot analysis of phospho-ERK, ERK, phospho-S6, S6, and actin 48 h hours after addition of doxycycline and either vehicle (DMSO control), MAPK/ERK inhibitor U0126 (U; 10 μM), or rapamycin (R; 15 nM). Panel **B**: Representative images of EPC monolayers with no Doxycycline (No Dox), plus Doxycycline, and either vehicle (DMSO control), MAPK/ERK inhibitor U0126 (10 μM), or rapamycin (15 nM). Scale bar = 200 μm. Panel **C**: Circularity index measurements for EPC-expressing $NRAS^{WT}$ and $NRAS^{Q61R}$ in Dox-containing media at 48 h and DMSO control (-), MAPK/ERK inhibitor U0126 (U; 10 μM), or rapamycin (R; 15 nM). Data are expressed in % change relative to No Dox control. One-way Anova followed by Tukey's test for multiple comparisons. ns: $p > 0.05$

implicated in the manifestation of vascular anomalies, and as such it will be a critical area for future discovery.

The mTOR inhibitory drug rapamycin has become a standard therapy for many patients with complex vascular anomalies; however, it often only produces a partial response and patients can rebound if therapy is withdrawn [21]. Hence, there is a great need for new therapeutic agents to be developed. Pre-clinical models for vascular anomalies are vital to identify new targets and test treatments. Therefore, in a proof-of-concept study, we evaluated whether a well-known MAPK/ERK inhibitor (U0126) or rapamycin prevented the shift to a spindle-shaped morphology in the $NRAS^{Q61R}$ mutant cells. The study clearly showed that U0126 prevented the spindle morphology shift in the mutant cells whereas rapamycin did not. A MEK inhibitor was effective in a recent KLA patient with a somatic mutation in Casitas B-lineage lymphoma (CBL) proto-oncogene [7]. In the future, these $NRAS^{Q61R}$ EPC models should prove useful to identify new therapeutic targets. Testing drug combinations will also be important as this may allow for lower doses to be used with improved efficacy and reduced side effects compared to one agent alone. In one KLA patient, multimodal therapy was much more effective than single treatment [22].

In summary, $NRAS^{Q61R}$ expression in human endothelial cells recapitulated many of the key characteristics seen in the lesions of vascular anomaly patients with RAS mutations. This provides support for $NRAS^{Q61R}$ as a key driver in the etiology of vascular anomalies. The in vitro and in vivo models reported can be used to gain a better understanding of the pathways driving the pathogenesis of mutant NRAS-induced diseases. These models should also facilitate pre-clinical testing of new treatments and combinational therapies.

Supplementary Information The online version contains supplementary material available at https://doi.org/10.1007/s10456-022-09836-7.

Acknowledgements Funding for this project was provided by the Lymphatic Malformation Institute (LMI) (T.D.L.), a gift from the Ferry Family (T.D.L.), and a Schmidlapp Women Career award (Cincinnati Children's Hospital Medical Center) (E.B.). Research reported in this manuscript was also supported by the National Heart, Lung, and Blood Institute, under Award Number R01 HL156866 (T.D.L) and Award Number R01 HL117952 (E.B.), part of the National Institutes of Health. The content is solely the responsibility of the authors and does not necessarily represent the official views of the National Institutes of Health. We thank the Veterinary Services, Confocal Core, and Viral Vector Core at Cincinnati Children's Hospital Medical Center for providing state-of-the-art services.

Author Contributions TDL and EB: conceived the project. TDL and EB: supervised the research. DP: generated the lentiviral constructs. PP: performed the NRAS EC infections, migration, and immunoblotting. SS: performed cell proliferation and 3D lumen formation assays and analysis. RK: performed the cell shape measurements and analysis. PP, JG, and EB: performed in vivo experiments, immunostaining, and analysis. EB: prepared the figures. TDL and EB: wrote the manuscript. PM, SS, PP, JG, RK, and DP: reviewed the manuscript.

Data availability The datasets generated during and/or analyzed during the current study are available from the corresponding author on reasonable request.

Declarations

Consent for publication The authors have no financial or non-financial interests that are directly or indirectly related to the work submitted for publication.

References

1. Degirmenci U, Wang M, Hu J (2020) Targeting aberrant RAS/RAF/MEK/ERK signaling for cancer therapy. Cells 9(1):198
2. Munoz-Couselo E et al (2017) NRAS-mutant melanoma: current challenges and future prospect. Onco Targets Ther 10:3941–3947
3. Queisser A, Boon LM, Vikkula M (2018) Etiology and genetics of congenital vascular lesions. Otolaryngol Clin North Am 51(1):41–53
4. Groesser L et al (2016) BRAF and RAS mutations in sporadic and secondary pyogenic granuloma. J Invest Dermatol 136(2):481–486
5. Lim YH et al (2015) Somatic activating RAS mutations cause vascular tumors including pyogenic granuloma. J Invest Dermatol 135(6):1698–1700
6. Barclay SF et al (2019) A somatic activating NRAS variant associated with kaposiform lymphangiomatosis. Genet Med. 21(7):1517–1524. https://doi.org/10.1038/s41436-018-0390-0
7. Foster JB et al (2020) Kaposiform lymphangiomatosis effectively treated with MEK inhibition. EMBO Mol Med 12(10):e12324
8. Ingram DA et al (2004) Identification of a novel hierarchy of endothelial progenitor cells using human peripheral and umbilical cord blood. Blood 104(9):2752–2760
9. Schneider CA, Rasband WS, Eliceiri KW (2012) NIH Image to ImageJ: 25 years of image analysis. Nat Methods 9(7):671–675
10. Nakatsu MN, Hughes CC (2008) An optimized three-dimensional in vitro model for the analysis of angiogenesis. Methods Enzymol 443:65–82
11. Schindelin J et al (2012) Fiji: an open-source platform for biological-image analysis. Nat Methods 9(7):676–682
12. Le Cras TD et al (2020) Constitutively active PIK3CA mutations are expressed by lymphatic and vascular endothelial cells in capillary lymphatic venous malformation. Angiogenesis 23(3):425–442
13. Cai Y et al (2019) Constitutive Active Mutant TIE2 Induces Enlarged Vascular Lumen Formation with Loss of Apico-basal Polarity and Pericyte Recruitment. Sci Rep 9(1):12352
14. Croteau SE et al (2014) Kaposiform lymphangiomatosis: a distinct aggressive lymphatic anomaly. J Pediatr 164(2):383–388
15. Limaye N et al (2015) Somatic activating PIK3CA mutations cause venous malformation. Am J Hum Genet 97(6):914–921
16. Crist AM et al (2019) Angiopoietin-2 inhibition rescues arteriovenous malformation in a smad4 hereditary hemorrhagic telangiectasia mouse model. Circulation 139(17):2049–2063
17. Li QF et al (2018) Activation of ras in the vascular endothelium induces brain vascular malformations and hemorrhagic stroke. Cell Rep 24(11):2869–2882

18. Li X et al (2019) Ponatinib combined with rapamycin causes regression of murine venous malformation. Arterioscler Thromb Vasc Biol 39(3):496–512
19. Fish JE et al (2020) Somatic gain of KRAS function in the endothelium is sufficient to cause vascular malformations that require MEK but not PI3K signaling. Circ Res 127(6):727–743
20. Homayun-Sepehr N et al (2021) KRAS-driven model of gorham-stout disease effectively treated with trametinib. JCI Insight 6(15):e149831
21. Adams DM et al (2016) Efficacy and safety of sirolimus in the treatment of complicated vascular anomalies. Pediatrics 137(2):1–10
22. Crane J et al (2020) Kaposiform lymphangiomatosis treated with multimodal therapy improves coagulopathy and reduces blood angiopoietin-2 levels. Pediatr Blood Cancer 67(9):e28529